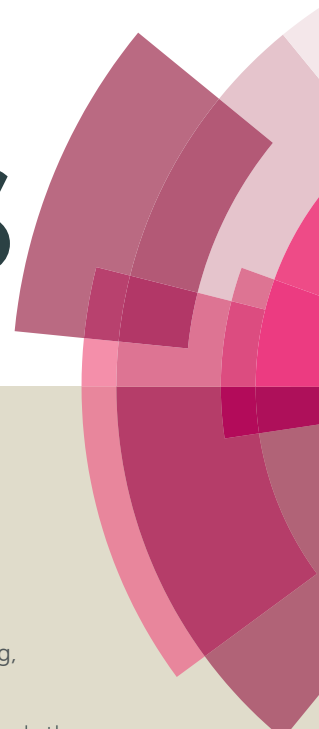


RSC Advances



This article can be cited before page numbers have been issued, to do this please use: G. tan, Z. Cheng, Y. QIU, W. Huang, H. Fan and B. Ren, *RSC Adv.*, 2016, DOI: 10.1039/C6RA02162J.



This is an *Accepted Manuscript*, which has been through the Royal Society of Chemistry peer review process and has been accepted for publication.

Accepted Manuscripts are published online shortly after acceptance, before technical editing, formatting and proof reading. Using this free service, authors can make their results available to the community, in citable form, before we publish the edited article. This *Accepted Manuscript* will be replaced by the edited, formatted and paginated article as soon as this is available.

You can find more information about *Accepted Manuscripts* in the [Information for Authors](#).

Please note that technical editing may introduce minor changes to the text and/or graphics, which may alter content. The journal's standard [Terms & Conditions](#) and the [Ethical guidelines](#) still apply. In no event shall the Royal Society of Chemistry be held responsible for any errors or omissions in this *Accepted Manuscript* or any consequences arising from the use of any information it contains.

Supercapacitors Based on Polyelectrolyte/Ferrocenyl-surfactant Complexes with High Rate Capability

Cite this: DOI: 10.1039/x0xx00000x

Guiping Tan,^a Zhiyu Cheng,^{*a} Yongfu Qiu,^{*a} Weiqing Huang,^a Hongbo Fan,^a Biye Ren,^b

Received 00th xxxxx 2016,
Accepted 00th xxxxx 2016

DOI: 10.1039/x0xx00000x

www.rsc.org/

Abstract: In this research, a composite of the Polyelectrolyte/Ferrocenyl-surfactant Complexes (PFSC) coated on carbon paper (CP) was applied as electrode materials for supercapacitors. The as-prepared composite possessed a specific capacitance as high as 214 F g⁻¹ calculated from discharge curve with current density 0.8 A g⁻¹ and this observation was deemed to originate from its ferrocenyl moieties. Furthermore, the specific capacitances calculated from cyclic voltammograms were 145 and 103 F g⁻¹ at potential scan rate 20 and 50 mV s⁻¹, which kept 77.6 % and 55.4 % of the corresponding value at 10 mV s⁻¹ (187 F g⁻¹). This suggested that the composite possessed good rate capability as a novel redox active electrode material for pseudo-capacitors. In a word, for the first time the composite PFSC/CP was reported as a promising electrode material for efficient supercapacitors.

Key words: Supercapacitor; Ferrocene; Polyelectrolyte-Surfactant Complexes

1. Introduction

Supercapacitors with high power and much longer shelf and cycle life than batteries have attracted great attention over the past few years.¹⁻³ Generally, electrical double layer capacitors (EDLCs) store energy in terms of electrical double-layer. To enhance their capacitances, a typical strategy is to utilize carbon electrodes with large surface areas and appropriate pore-size distributions. Carbon materials including activated carbon, carbon nanotube, carbon spheres, porous carbon and graphene are usually used as electrodes.¹⁻⁹ In comparison with EDLCs, pseudo-capacitors are described in terms of faradic charge transfer originating by a very fast sequence of reversible faradaic redox, electrosorption or intercalation processes on the surface of suitable electrodes. They are more attractive due to their higher capacitance and energy density through Faradic reactions.^{1-3,10} Manganese dioxide (MnO₂) is considered as one of the most promising pseudo-capacitive materials because of its superior capacitance (> 1370 F/g), environment friendly and cost-effective characteristics.¹¹ However, pseudo-capacitors based on MnO₂ often provide poor rate capability due to its low electrical conductivity (10⁻⁵ - 10⁻⁶ S cm⁻¹).^{12,13}

In order to enhance rate capability for pseudo-capacitors, other electrode materials with redox couple could be considered. Ferrocene and its derivatives have been used as a family of fascinating organometallic electron mediators because of their redox properties. They usually serve as the electron transfer media between redox matrix and electrode in electrochemical and biological sensors.¹⁴⁻¹⁷ Therefore, Polyelectrolyte/Ferrocenyl-surfactant complexes (PFSC) are expected to be used as electrode materials in pseudo-capacitors, due to their excellent redox properties originating from that the generated electrons on ferrocenyl groups will be conducted and separated through self-assembled and -organized 3D structures.

In this research, The PFSC was used as an electrodes material for pseudo-capacitors and the commercial carbon papers was used as substrates and current collectors. The PFSC were prepared *via* the ionic self-assembly of sodium poly(styrenesulfonate) (PSS) and (11-ferrocenylundecyl)-trimethylammonium bromide (FTMA) in aqueous solution. PFSC film was anchored onto the carbon paper (CP) to form a composite PFSC/CP through a solution casting technique. The as-prepared composite possesses a specific

ARTICLE

capacitance as high as 214 F g^{-1} calculated from discharge curve with current density 0.80 A g^{-1} . Furthermore, the specific capacitances calculated from cyclic voltammograms are 145 and 103 F g^{-1} at potential scan rate 20 and 50 mV s^{-1} , which retain 77.6 % and 55.4 % of the corresponding value at 10 mV s^{-1} (187 F g^{-1}). This indicates that the PFSC/CP composite possesses good rate capability as a novel redox active electrode material for pseudo-capacitors.

2. Experimental

2.1 Materials.

Sodium poly(styrenesulfonate) (PSS, Aldrich, $M_w = 70,000$) was used as received. 11-Bromoundecyl ferrocene was synthesized according to our previous report.¹⁸ All the other chemicals were analytical reagents and purified according to the standard procedures. Water used in all experiments was deionized and filtrated by a Millipore purification apparatus with resistivity more than $18.0 \text{ M}\Omega\text{-cm}$.

2.2 Synthesis of (11-ferrocenylundecyl)trimethylammonium bromide (FTMA).

The ferrocenyl surfactant FTMA was synthesized according to the literature procedure.¹⁹ The target product FTMA was synthesized through nucleophilic substitution reaction between 11-bromoundecyl ferrocene and trimethylamine. The synthetic routes and $^1\text{H NMR}$ spectrum of the FTMA measured in CDCl_3 are shown in Fig. 1 and Fig. 2, respectively. The characterization data are listed as follows, $^1\text{H NMR}$ (CDCl_3 , TMS) δ (ppm) 4.11 (m, 9H, $H(\text{Cp})$), 3.54 (t, 2H, $-\text{CH}_2-\text{N}-$), 3.40 (s, 9H, $(\text{CH}_3)_3-\text{N}-$), 2.23 (t, 2H, $\text{Cp}-\text{CH}_2-$), 1.69 (m, 2H, $-\text{CH}_2-\text{CH}_2-\text{N}-$), 1.44-1.23 (m, 16H, $\text{Cp}-\text{CH}_2-\text{CH}_2-(\text{CH}_2)_8-$). FT-IR (KBr) ν 3092, 1466, 1105, 1000, and 816 cm^{-1} (Characteristics of ferrocene groups absorption peaks), 2923 cm^{-1} ($\nu_{\text{as}} \text{CH}_2$), 2852 cm^{-1} ($\nu_{\text{s}} \text{CH}_2$), 1631 cm^{-1} ($\nu_{\text{s}} = \text{N}^+=$).

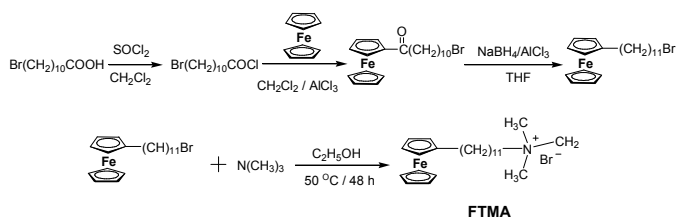


Fig. 1 Synthesis route of ferrocenyl surfactant FTMA.

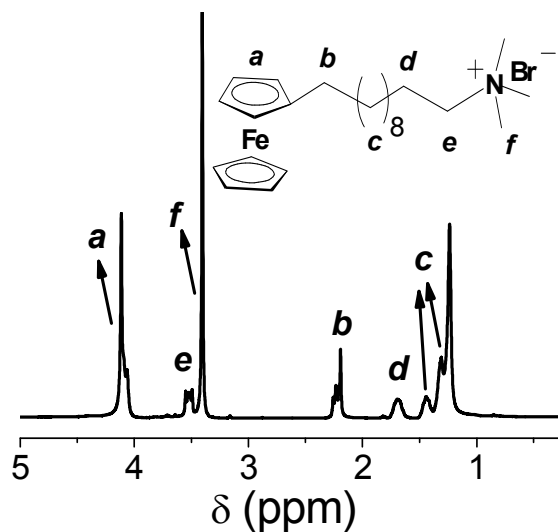


Fig. 2 $^1\text{H NMR}$ spectrum of the FTMA measured in CDCl_3 .

2.3 Preparation of PFSC and its film

The PFSC was prepared according to the following procedure: 239 mg (0.5 mmol) of FTMA was dissolved in 5 mL of water at about $80 \text{ }^\circ\text{C}$ and slowly added dropwise into 5 mL of boiling water containing 103 mg (0.5 mmol of repeat unit) of PSS under stirring. The yellow precipitate was separated by filtration, washed several times with hot water, and dried for 76 h under vacuum at $40 \text{ }^\circ\text{C}$. The chemical structure of PFSC and its electron transfer reaction equation were illustrated in Fig. 3. For preparation of complex films, the chloroform solution of the PFSC with $2 \times 10^{-5} \text{ mol L}^{-1}$ (counted for the ferrocenyl surfactant, the following is the same) was coated on a quartz glass at room temperature and dried for 48 h under vacuum at $40 \text{ }^\circ\text{C}$.

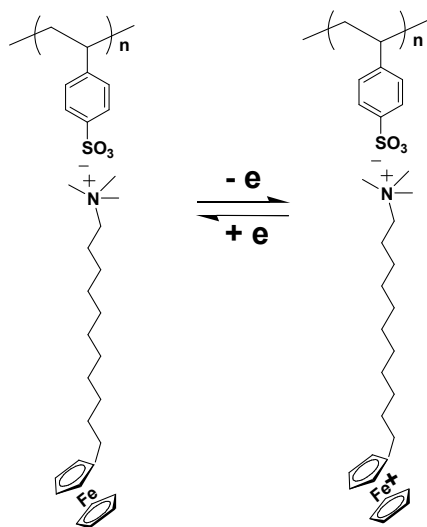


Fig. 3 Chemical structure of PFSC and its electron transfer reaction.

2.4 Preparation of PFSC/CP

As a general procedure, carbon paper (CP) electrode was sonicated in ethanol and doubly distilled water for 30 s, respectively. A freshly cleaned CP electrode was soaked in a solution of 0.07 mol L⁻¹ PFSC in chloroform for 10s. A small bottle was sealed tightly covering the electrode to serve as a closed chamber to make chloroform evaporate slowly. The CP electrode modified with the PFSC film (denoted as PFSC/CP) was then dried in N₂ atmosphere at room temperature. The loading mass of the PFSC for PFSC/CP electrode are 1.0 mg cm⁻².

2.5 Characterization

Wide-angle X-ray diffraction (WAXD) and small-angle X-ray scattering (SAXS) measurements of the complex film were performed in transmission geometry with an X'pert PRO diffractometer (40 KV and 40 mA) using Cu K_α radiation (wavelength $\lambda = 0.154$ nm) at room temperature. The 2θ ranged from 10° to 30° for WAXD and the scattering vector s ranged from 0.1 to 1.5 nm⁻¹ for SAXS, where $s = (2/\lambda) \sin \theta$. The scan step was 0.01° in 2θ with counting time of 1 s/step. Thermogravimetry (TG) was measured with a Netzsch TG 209 under nitrogen atmosphere at heating rate of 10°C min⁻¹ starting from room temperature up to

750 °C. The differential scanning calorimetry (DSC) was carried out with 4-5 mg of sample in a 6 mm aluminum pan on a Netzsch DSC 204 under nitrogen atmosphere at heating or cooling rate of 10°C min⁻¹ following the temperature sequence as room temperature → 130 °C → -45 °C → 130 °C. Polarized optical microscope of Zeiss Axiophot was used with a Linkam hot stage. ¹H NMR spectrum was obtained in CDCl₃ solution on a Varian INOVA 500NB spectrometer. UV-visible absorbance was measured with a Hitachi UV-3010 spectrophotometer. Polarized optical microscope (POM) of Zeiss Axiophot was used with a Linkam hot stage. The sample was heated from room temperature to 110 °C to remove the heat history and then cooled to room temperature and subsequently heated to 110 °C again at the rate of 10 °C min⁻¹. The POM photos of the PFSC were taken at 25 and 100 °C for smetic A phase and isotropic state, respectively. Cyclic voltammetry (CV) and galvanostatic charge/discharge measurements were performed in a three-electrode system using a CHI 440a electrochemical work station, with 0.1 M Na₂SO₄ as the electrolyte solution. The composite PFSC/CP with a projection area of 0.2 cm² were used as the working electrode, Ag/AgCl (3.0 M KCl) and a Pt wire as the reference and counter electrodes, respectively. The electrochemical impedance spectroscopy (EIS) measurements were carried out by using a potentiostat (EG&G, M2273), the frequency range analyzed was 0.1 Hz to 100 Hz with AC amplitude of 10 mV.

2.6 Calculation

The specific capacitance for the electrode can be calculated as, $C = \frac{1}{m\nu(U_c - U_a)} \int_{U_a}^{U_c} I(U) dU$, where C is the specific capacitance (F g⁻¹), m is the mass of PFSC (g), ν is the potential scan rate (V s⁻¹), $U_c - U_a$ is the sweep potential range during (U) discharging branch and $I(U)$ denotes the response current density (A g⁻¹). In addition, gravimetric capacitance for a single electrode was calculated from the discharge curve in the three-electrode cell by the equation, $C_{single} = \frac{I\Delta t}{\Delta V}$, where I is the constant current (A g⁻¹), Δt is the discharge time, ΔV is the voltage range during the discharge process.²⁰

3. Results and Discussion

3.1 Structural Analysis.

WAXD and SAXS measurements were performed and shown in Fig. 4 for PFSC film at room temperature. In the wide angle range (Fig. 4A), only a broad peak appeared at $2\theta \approx 17.7^\circ$, corresponding to the distance between the conformationally disordered alkyl chains. This indicated the non-crystalline structure in the solid PFSC at room temperature.

In the small angle range (Fig. 4B), there were two peaks at the equidistant position in s scale as 1:2 (the scattering vectors s of 0.32 and 0.63 nm^{-1} correspond to the long period of $d_{001} = 31.3$ and $d_{002} = 15.8 \text{ \AA}$, respectively.), indicating the typical lamella mesomorphous structure for PFSC. The results were similar to that proposed by Antonitti *et al.* for the complexes of PSS and different alkyltrimethylammonium derivatives.²¹ They suggested that the lamella was composed of two layers as polyions (polyelectrolyte and ionic head groups) and alkyl chains (tails) and the long period depends on the length and orientation of alkyl chains of surfactant. With the results of Antonitti *et al.*²¹, the thickness of the alkyl tail layer was estimated to be 17.3 \AA for PFSC. The value was close to the tail length ($\sim 18.8 \text{ \AA}$) calculated for the stretched corresponding alkyl chains with the given carbon numbers and ferrocenyl groups ($\sim 5 \text{ \AA}$), because the increment of one carbon is about 1.25 \AA to the long period for a completely stretched alkyl chain if the chain was perpendicular to the lamella.²¹ Hence, the surfactant tails were interdigitately arranged in a monolayer in the complexes. The possible structure of PFSC film is schematically illustrated in Fig. 4C.

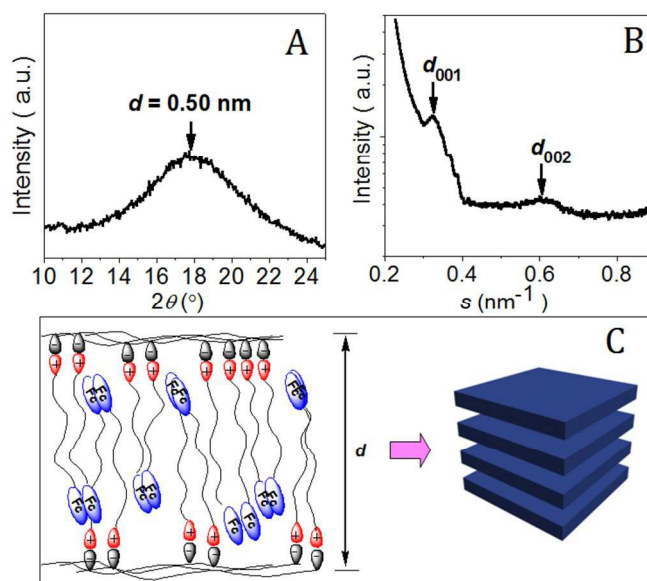


Fig. 4 WAXD (A) and SAXS (B) patterns of the PFSC, where $s = (2/\lambda) \sin \theta$; (C) Possible structure model of the PFSC.

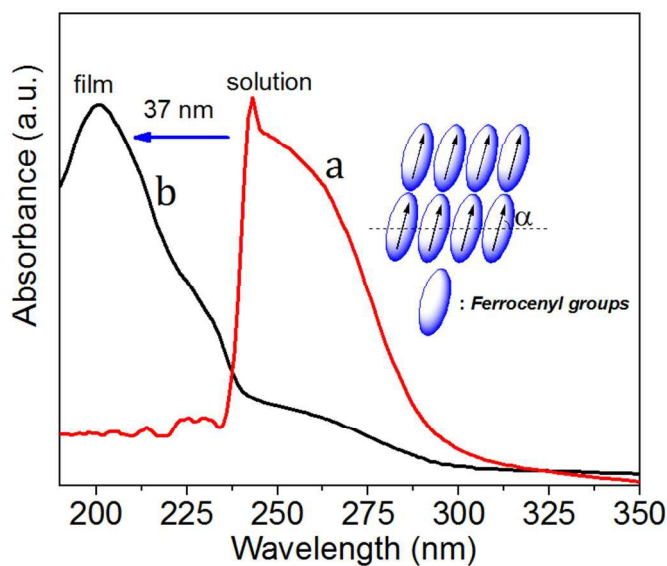


Fig. 5 UV-vis spectra of the PFSC in chloroform solution (a) and solid film (b). Inset is the H-aggregate model for ferrocenyl moieties in the PFSC.

The chromophores could stack in parallel and form an angle α between the chromophore transition dipoles and the line passing through the dipole centers. For the H-aggregate α was greater than 54.7° and for the J-aggregate α was less than 54.7° .²² Fig. 5 showed UV-vis spectra of the PFSC in film and in chloroform solution. There were usually two peaks at *ca.* 240 and 440 nm in the UV-vis spectrum for the ferrocene and its derivatives, but the latter was very

weak. As seen from Fig. 5, the maximum absorbance of the PFSC in chloroform solution appeared at about $\lambda_{\max} = 240$ nm, resulting from the π - π^* electron transition of ferrocenyl moieties. In contrast, the PFSC film presented λ_{\max} at about 203 nm, which blue-shifts about 37 nm from $\lambda_{\max} = 240$ nm for the PFSC in solution, suggesting the H-aggregate among ferrocenyl moieties causing an increase in the π - π^* transfer energy of cyclopentadiene, similar to that reported by Shen et al.²³ on the N,N-dimethylferrocenyl methylhexadecylammonium (Fc16) bromide containing LB film. According to exciton-coupling theory developed by Kasha et al.,²² noncovalent dimerization of molecules within an aggregate lowers the degeneracy of its excited electronic state compared to the uncoupled monomers. For H-aggregates, the higher electronic state carries all of the oscillating strength while transition to the lower electronic (exciton) state is forbidden. As the result, the absorption of the aggregate is blue-shifted in accordance with Kasha's rules.²⁴ The present behavior suggests that the ferrocenyl moieties of the PFSC film would form a close molecular packing as the H-aggregate, i.e., the cyclopentadienyl rings of ferrocenyl moieties are parallel to each other and tilted in the complex film organized by the ordered packing structure of alkyl tails. The H-aggregate among ferrocenyl moieties of PFSC film is also schematically illustrated in Fig. 4C.

3.2 Thermal Properties and POM Analysis.

In order to understand the nature of PFSC, we determined the thermal properties with TG and DSC. TG thermograms in Fig. 6A demonstrate that there is no significant weight-loss up to 220 °C for PFSC, indicating their high thermal stability. PFSC exhibited a two-step weight-loss process over 220-750 °C. The degradation temperature T_{d1} corresponding to the first maximum weight-loss rate for the PFSC is 338 °C, while degradation temperature T_d for the surfactants FTMA is approximately 265 °C. This indicates that the thermal stability of the complex is significantly enhanced when compared with the corresponding pure surfactant as the result of strong electrostatic interaction between $-\text{SO}_3^-$ (from PSS) and $>\text{N}^+$ (from ferrocenyl surfactant). The second maximum weight-lost at about 460 °C is attributed to the degradation of PSS polymer in the complex. The corresponding degradation temperature T_{d2} increases

from 442 °C for the pure PSS to 460 °C for the complexes. In a word, according to the higher degradation temperature, the complexes showed higher thermal stability compared with their components due to the ionic interaction.

Only a weak endothermic peak at 93.6 °C and no glass transition during the second heating run were detected from the DSC trace above -45 °C for PFSC (Fig. 6B). There was no glass transition in complexes due to the stiffening of the PSS chains resulting from arrangement of the bound FTMA. We considered that the complexes were in the liquid crystal state below T_i (93.6 °C) corresponding to the transition from liquid crystal to isotropic phase as further verified with POM. Fig. 6C and D illustrated POM photographs of the complexes taken at 25 and 100 °C, respectively. PFSC exhibited a random birefringent polygon-like texture below T_i (Fig. 6C). The oriented texture was observed after sheared and disappeared when temperature was above T_i (Fig. 6D). Combining with the finding from WAXD and SAXS, PFSC was ionic thermotropic smectic A phase below T_i .

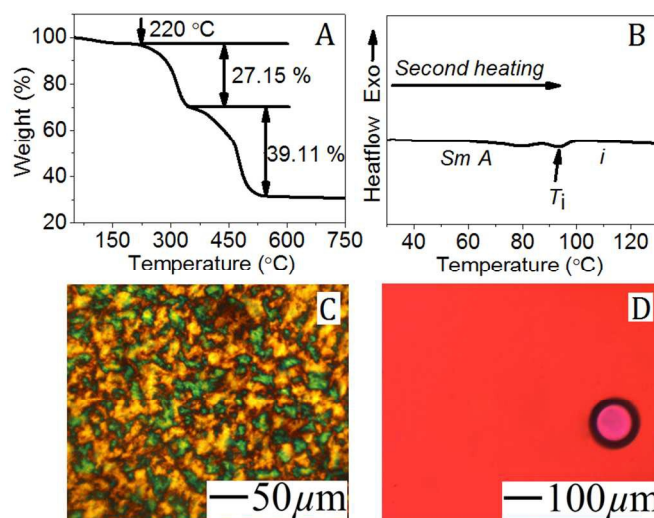


Fig. 6 (A) TG thermogram of the PFSC; (B) DSC traces of PFSC during the second heating run at the rate of 10 °C min⁻¹; Polarized optical micrographs for PFSC: (C) smectic A phase at 25 °C, (D) isotropic phase at 100 °C.

3.3 Cyclic Voltammetry and Galvanostatic Charge/discharge Measurements

In order to examine the electrochemical behaviors of our samples, their cyclic voltammograms and galvanostatic charge/discharge results are shown in Fig.7. In Fig. 7A, the CV curve of CP with quasi-rectangular was observed exhibiting their double-layer capacitance behaviors, and a couple of redox peaks were examined from CV curve of PFSC/CP, indicating this composite with obviously redox behaviours of PFSC, which similar with other ferrocenyl-modified materials.

To investigate the electrochemical effect of PFSC on the composite PFSC/CP, the areal capacitances for CP and PFSC/CP at scan rate 10 mV s^{-1} are calculated as 38 and 60 mF cm^{-2} shown in Fig. 7B. It should be noted that their areal capacitances calculated using the equation: $C = \frac{1}{S(U_c - U_a)} \int_{U_a}^{U_c} I(U) dU$,²⁰ where S is the plane area of sample. The calculated results suggest that PFSC anchored onto CP has dramatically increased the areal capacitances.

The typical CV curves for PFSC/CP at different potential scan rates are given in Fig. 7C and they all have a couple of redox peaks at 10, 20 and 50 mV s^{-1} potential scan rates. This indicates that the composite PFSC/CP has redox properties and excellent rate capabilities.¹ While, the CV curves deviating from redox peaks shape upon potential scan rates higher than 50 mV s^{-1} imply that the CV processes were controlled by the relatively slow diffusion of ions in electrolyte such as Na^+ , SO_4^{2-} , H^+ and OH^- or by these ions diffusion in the two-stage structure of PFSC/CP, and accordingly some PFSC materials under the interface does not make a remarkable contribution for the capacitance performance of pseudocapacitors.^{25,26} The specific capacitances of PFSC/CP calculated from cyclic voltammograms are shown in Fig. 7D. The decrease of the specific capacitances for PFSC/CP with the increasing potential scan rates can be observed. Their specific capacitances at scan rates of 20 and 50 mV s^{-1} are 145 and 103 F g^{-1} respectively, which retain 77.6% and 55.4% of the corresponding value 187 F g^{-1} at 10 mV s^{-1} .

This implies that the composite PFSC/CP has excellent rate capability as an electrode material for supercapacitors.

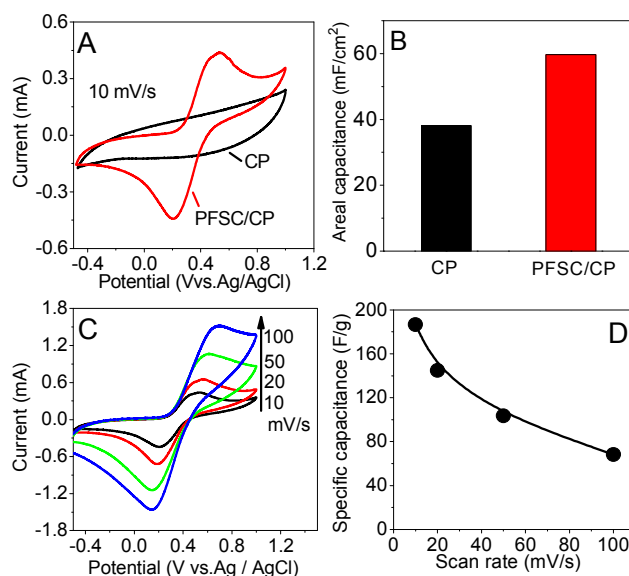


Fig. 7 (A) Cyclic voltammograms collected at scan rate 10 mV s^{-1} for CP and PFSC/CP; (B) Calculated areal capacitances for CP and PFSC/CP at scan rate 10 mV s^{-1} ; (C) CV collected at different scan rates for PFSC/CP; (D) Calculated areal capacitances of the PFSC/CP from CV as a function of scan rate. (All the data of CV was measured with $0.1 \text{ M Na}_2\text{SO}_4$ as the electrolyte solution.)

The PFSC/CP exhibiting the best supercapacitor performance was confirmed by the galvanostatic charge/discharge measurements in the three-electrode system. In Fig. 8A, the charge-discharge curves for PFSC/CP at different current densities generally show symmetrical and linear profiles upon current densities larger than 2.4 A g^{-1} , suggesting its excellent supercapacitive behaviors. However, once current densities lower than 1.6 A g^{-1} , an obvious platform could be clearly observed in charge or discharge curve, which is due to the reversibility reaction of oxidation/reduction for the ferrocenyl motifs in the composite PFSC.

The typically specific capacitances for a single electrode calculated from the discharge branches are shown in Fig. 8B. Discharging at varied specific current densities 0.8, 1.6, 2.4, and 3.2

A g^{-1} , the corresponding specific capacitances are 214, 132, 62 and 31 F g^{-1} . This also implies the excellent supercapacitive behaviors of the composite PFSC/CP in terms of superior reversible redox reactions taking place within the sample. At a current density 0.80 A g^{-1} , the calculated specific capacitance for PFSC/CP is 214 F g^{-1} . This value is close to 250.0 F g^{-1} for the flat MnO_2 electrode.²⁷ In addition to high rate capability, the cycle life test over 2000 cycles for PFSC/CP was performed at a current density of 3.2 A g^{-1} and the results in Fig. 9A showed that the capacitance decay over 2000 cycles is $\sim 12\%$, indicating its long cycle life.

The power capability of supercapacitors is primarily dependent on their resistance, according to the equation $P_{sc} = 9(1 - EF)V_0^2/16R_{sc}$, where V_0 is the rated voltage of the supercapacitor, R_{sc} is the resistance of the supercapacitor and EF is the efficiency of the supercapacitor.²⁸ Usually, the resistance response is measured in the pulsed mode of operation for determining the peak useable power capability. The Nyquist-type impedance spectra in Fig. 9B show that only upward sloping lines for CP and PFSC/CP electrodes, which suggesting that both electrodes have low diffusion resistance and exhibit high power capacitive performance.^{29,30}

To design high performance supercapacitors utilizing pseudo-capacitance, the electronic conductivity and redox property of electrode materials are the two facts playing the key roles in affecting the electrochemical behaviours. In our case, the carbon paper has well hydrophobicity leading to its strong interaction with the deposited PFSC, thus with low resistance response for electrodes. In addition, the redox properties of PFSC are advantageous to improve the specific capacitance for the electrode. In brief, the composite PFSC/CP was reported for the first time as a promising electrode material for efficient supercapacitors.

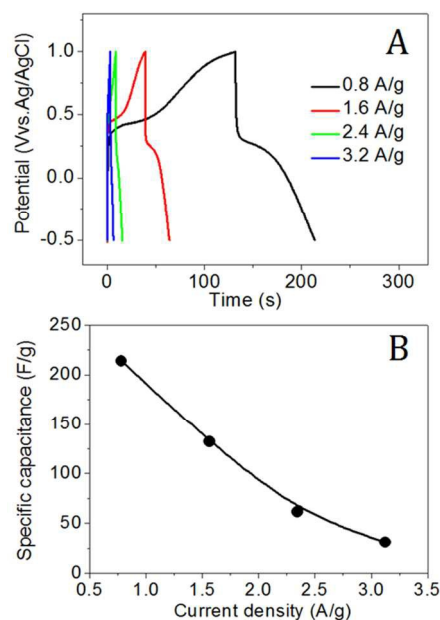


Fig. 8 (A) Charge-discharge curves at various current densities for PFSC/CP; (B) Areal capacitance calculated based on charge-discharge curves from plot (A) as a function of current density.

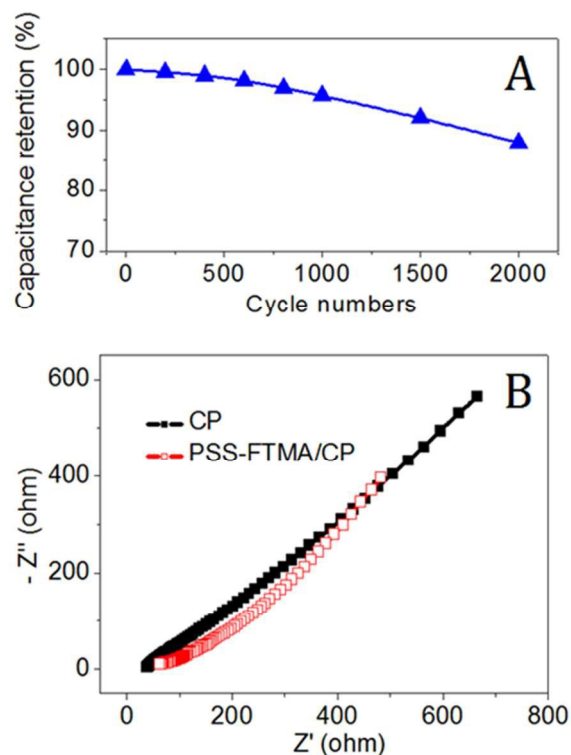


Fig. 9 (A) Capacitance retention test over 2000 cycles at a current density of 1.0 A g^{-1} for PFSC/CP; (B) Nyquist electrochemical impedance spectra of CP and PFSC/CP.

4. Conclusion

In summary, before preparing the composite PFSC/CP, the redox active polyelectrolyte-surfactant complexes PFSC were prepared *via* the ionic self-assembly firstly. The PFSC complex exhibited an ordered interdigitated monolayer mesomorphous structure with the long period of $d = 3.13$ nm, and was in the ionic thermotropic liquid crystal SmA state at room temperature. Interestingly, in the complex film, the ferrocenyl moieties formed H-aggregation. Furthermore, the complexes showed higher thermal stability compared with their components. The electrochemical behaviors of the composite PFSC/CP were characterized by cyclic voltammograms and galvanostatic charge/discharge. The composite PFSC/CP possessed a specific capacitance as high as 214 F g^{-1} . Their specific capacitances at scan rates of 20 and 50 mV s^{-1} are 145 and 103 F g^{-1} respectively, which retain 77.6% and 55.4% of the corresponding value 187 F g^{-1} at 10 mV s^{-1} . The high capacitance and high rate capability of our supercapacitors originated from the low resistance response and the very fast reversible faradaic redox of the composite PFSC/CP. In a word, the composite PFSC/CP is reported for the first time, and it is a promising electrode material for building up an efficient supercapacitor.

Acknowledgements

The work described in this paper was supported by the National Natural Science Foundation of China (No. 21274047), the characteristic innovation project for natural science in Guangdong provincial key platform and major scientific research projects for colleges and universities (2015KTSCX139), foundation for the Excellent Young Teachers in Higher Education Institutions of Guangdong (Yongfu Qiu, 2014), the Natural Science Foundation of Guangdong Province (No. 2015A030313651, 2015A030310235), the Foundation of the Department of Education of Guangdong Province (No. 2014KQNCX218). Thanks to Qiu Yan (1941308558@qq.com) for her linguistic assistance during the preparation of this manuscript.

Notes and references

^a College of Chemistry and Environmental Engineering, Guangdong Engineering and Technology Research Center for Advanced Nanomaterials, Dongguan University of Technology, Guangdong 523808, P. R. China.

^b Research Institute of Materials Science, South China University of Technology, Guangzhou 510640, P. R. China.

* Author to whom any correspondence should be addressed. Tel/fax: +86 769 2286 1232, E-mail address: mszycheng@scut.edu.cn or qiuyl1979@foxmail.com.

- 1 G. P. Wang, L. Zhang and J. J. Zhang, *Chem. Soc. Rev.*, 2012, **41**, 797-828.
- 2 D. S. Yu, Q. H. Qian, L. Wei, W. C. Jiang, K. L. Goh, J. Wei, J. Zhang and Y. Chen, *Chem. Soc. Rev.*, 2015, **44**, 647-662.
- 3 X. Peng, L. L. Peng, C. Z. Wu and Y. Xie, *Chem. Soc. Rev.*, 2014, **43**, 3303-3323.
- 4 Y. W. Zhu, S. Murali, M. D. Stoller, K. J. Ganesh, W. W. Cai, P. J. Ferreira, A. Pirkle, R. M. Wallace, K. A. Cychosz, M. Thommes, D. Su, E. A. Stach and R. S. Ruoff, *Science*, 2011, **332**, 1537-1541.
- 5 P. H. Jampani, O. Velikokhatnyi, K. Kadakia, D. H. Hong, S. S. Damle, J. A. Poston, A. Manivannan and P. N. Kumta, *J. Mater. Chem. A*, 2015, **3**, 8413-8432.
- 6 X. L. Chen, H. J. Lin, P. N. Chen, G. Z. Guan, J. Deng and H. S. Peng, *Adv. Mater.*, 2014, **26**, 4444.
- 7 A. M. Abdelkader, *J. Mater. Chem. A*, 2015, **3**, 8519-8525.
- 8 W. Q. Tian, Q. M. Gao, Y. L. Tan, K. Yang, L. H. Zhu, C. X. Yang and H. Zhang, *J. Mater. Chem. A*, 2015, **3**, 5656-5664.

RSC Advances

- 9 J. H. Shi, X. C. Li, G. H. He, L. Zhang and M. Li, *J. Mater. Chem. A*, 2015, **3**, 20619-20626.
- 10 K. Zhang, X. P. Han, Z. Hu, X. L. Zhang, Z. L. Tao and J. Chen, *Chem. Soc. Rev.*, 2015, **44**, 699-728.
- 11 Z. B. Lei, J. T. Zhang and X. S. Zhao, *J. Mater. Chem.*, 2012, **22**, 153-160.
- 12 F. Cao, Y. M. Liu, B. L. Chen, L. F. Fei, Y. Wang and J. K. Yuan, *Electrochim. Acta*, 2012, **81**, 1-7.
- 13 S. W. Lee, J. Kim, S. Chen, P. T. Hammond and Y. Shao-Horn, *ACS Nano*, 2010, **4**, 3889-3896.
- 14 M. J. Langton and P. D. Beer, *Accounts Chem. Res.*, 2014, **47**, 1935-1949.
- 15 F. Li, Y. Q. Yu, Q. Li, M. Zhou and H. Cui, *Anal. Chem.*, 2014, **86**, 1608-1613.
- 16 K. W. Ren, J. Wu, F. Yan, Y. Zhang and H. X. Ju, *Biosens. Bioelectron.*, 2015, **66**, 345-349.
- 17 C. Arivazhagan, R. Borthakur and S. Ghosh, *Organometallics*, 2015, **34**, 1147-1155.
- 18 C. Li, B. Ren, Y. Zhang, Z. Cheng, X. Liu and Z. Tong, *Langmuir*, 2008, **24**, 12911-12918.
- 19 T. Saji, K. Hoshino, Y. Ishii and M. Goto, *J. Am. Chem. Soc.*, 1991, **113**, 450-456.
- 20 J. Yan, Z. J. Fan, T. Wei, J. Cheng, B. Shao, K. Wang, L. P. Song and M. L. Zhang, *J. Power Sour.*, 2009, **194**, 1202-1207.
- 21 M. Antonietti, J. Conrad and A. F. Thünemann, *Macromolecules*, 1994, **27**, 6007-6011.
- 22 M. Kasha, *Molecular Excitons in Small Aggregates*, Plenum Press, New York, 1976.
- 23 Y. Shen, B. Xia, A. Xie and Y. Tang, *Colloid Surf. A*, 2005, **252**, 21-25.
- 24 A. Chowdhury, L. Yu, I. Raheem, L. Peteanu, L. A. Liu and D. J. Yaron, *J. Phys. Chem. A*, 2003, **107**, 3351-3362.
- 25 S. M. Zhu, H. S. Zhou, M. Hibino, I. Honma and M. Ichinara, *Adv. Funct. Mater.*, 2005, **15**, 381-386.
- 26 R. K. Sharma, H. S. Oh, Y. G. Shul and H. Kim, *Physica B*, 2008, **403**, 1763-1769.
- 27 Y. C. Qiu, Y. H. Zhao, X. W. Yang, W. F. Li, Z. H. Wei, J. W. Xiao, S. F. Leung, Q. F. Lin, H. K. Wu, Y. G. Zhang, Z. Y. Fan, S. H. Yang, *Nanoscale*, 2014, **6**, 3626-3631.
- 28 A. Burke, *J. Power Source*, 2000, **91**, 37-50.
- 29 Z. Gui, H. L. Zhu, E. Gillette, *ACS Nano*, 2013, **7**, 6037-6046.
- 30 C. W. Huang, C. A. Wu, S. S. Hou, *Adv. Funct. Mater.*, 2012, **22**, 4677-4685.

Supercapacitors Based on Polyelectrolyte/Ferrocenyl-surfactant Complexes with High Rate Capability

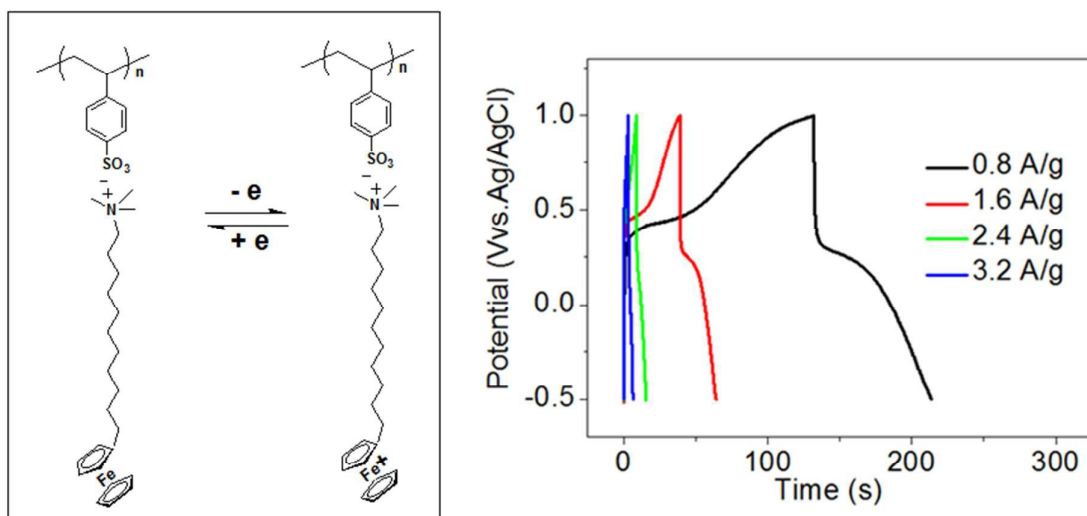
Guiping Tan,^a Zhiyu Cheng,^{*a} Yongfu Qiu,^{*a} Weiqing Huang,^a Hongbo Fan,^a Biye Ren,^b

^a College of Chemistry and Environmental Engineering, Guangdong Engineering and Technology Research Center for Advanced Nanomaterials, Dongguan University of Technology, Guangdong 523808, P. R. China.

^b Research Institute of Materials Science, South China University of Technology, Guangzhou 510640, P. R. China.

*Author to whom any correspondence should be addressed. Tel/fax: +86 769 2286 1232, E-mail address: qiuyf1979@foxmail.com or mszycheng@scut.edu.cn.

Table of Content



The composite PFSC/CP was reported as a promising electrode material for efficient supercapacitors for the first time.